CrystEngComm

Accepted Manuscript

This article can be cited before page numbers have been issued, to do this please use: A. Delledonne, M. Orlandini, F. Terenziani, P. P. Mazzeo, A. Bacchi, L. Carlucci, A. Comotti, J. Perego and P. Pelagatti, *CrystEngComm*, 2023, DOI: 10.1039/D3CE00087G.

ROYAL SOCIETY OF CHEMISTRY

rsc.li/crystengcomm

View Article Online
DOI: 10.1039/D3CE00087G

ARTICLE

Luminescent properties of mixed-ligand MOFs containing fluorene scaffolds functionalized with isonicotinoyl arms

Received 00th January 20xx,
Accepted 00th January 20xx

DOI: 10.1039/x0xx00000x

Andrea Delledonne,[a] Martina Orlandini,[a] Francesca Terenziani,[a]* Paolo Pio Mazzeo,[a] Alessia Bacchi,[a] Lucia Carlucci,[b] Angiolina Comotti,[c] Jacopo Perego[c] and Paolo Pelagatti[a,d]*

Solvothermal reactions between three bis-pyridine-bis-amide ligands containing a fluorene scaffold bearing different substituents on the C9 position (CH_2, **1;** CMe_2, **2**; C=O, **3**) with 2,6-naphthalenedicarboxylic acid (H_2ndca) and $Zn(NO_3)_2{\cdot}6H_2O$, led to the isolation of three new microporous mixed-ligand MOFs (**PUM310**, containing **1**; **PUM310Me$_2$**, containing **2**; **PUM310CO**, containing **3**). The structural characterization conducted by X-ray quality single crystals revealed in all cases parallel polycatenated frameworks of thick layers, corresponding to the topological type 5,6L18. The entangled nets contain complete and truncated Zn-paddle-wheels. In the truncated paddle-wheel a pyridine of the bis-amide linker has been replaced by a DMF molecule. Solvent removal leads to framework rearrangement, as evidenced by XRPD analysis performed on desolvated **PUM310**, with consequent framework shrinkage as also evidenced by volumetric adsorption analyses. The three MOFs are fluorescent in the solid state. The optical spectra are indicative of a Förster resonance energy transfer (FRET) involving ndca^{2-} as excitation energy donor and the bis-pyridine linkers as acceptors, with a FRET efficiency close to 100% in the case of **PUM310CO**.

Introduction

Although more than twenty years have passed since the pioneering work by Yaghi,[1] Metal-Organic-Frameworks (MOFs) are still attracting a tremendous scientific interest due to their high crystallinity, high porosity and high modularity.[2–4] MOFs are potentially porous coordination networks composed by metal nodes, often reported as Secondary-Building-Units (SBUs), and polytopic linkers.[5] The crystallinity of MOFs and then the knowledge of their precise crystalline structure, enables the design of new architectures and the development of new functional materials that make MOFs highly attractive in several applications, such as gas storage and separation,[6–10] guest-inclusion,[11–15] development of electronic materials,[16,17] food[18] and environmental[19] control and heterogeneous catalysis.[20–23] Among the physical properties that can be imparted to MOFs, luminescence covers a prominent role for the development of responsive crystalline materials. Indeed, luminescent MOFs (LMOFs), first reported in 2002,[24] are well documented in literature as sensors[25–27] or as light emitters[28–32] or for biological applications.[33] Luminescence in MOFs can originate from extended π-conjugated organic linkers used to connect the different SBUs (linker-based fluorescence),[26] or from the metal centers (metal-based fluorescence), when the SBUs are formed by suitable metal clusters[30–32,34–37] or lanthanide ions.[38] Alternatively, MOFs can become luminescent by hosting fluorescent guests into their intrinsically porous structure.[39,40] Several examples of LMOFs are related to mixed-ligand MOFs.[41,42] This class of multicomponent materials derives from the simultaneous incorporation in the framework of two distinct linkers.[43] It follows a widening of the number of functional groups that can be installed in the framework and, in turn, the number of architectures achievable by synthesis. Hence, the possibility of finely tuning the properties of the final materials.[44–48] In the last years we have directed our attention on Zn-containing mixed-ligand MOFs where one of the two linkers is constituted by a polyaromatic scaffold functionalized with bis-isonicotinoyl arms (Scheme 1), while the other is a linear dicarboxylate linker, such as 4,4'-biphenyldicarboxylate or 2,6-naphthalenedicarboxylate. These MOFs, grouped under the acronym PUM (Parma University Materials), have shown propensity for inclusion of organic guests[49–52] and CO_2 adsorption.[53]

Recently, we have reported on the solution and solid state luminescent properties of the three bis-isonicotinoyl linkers containing fluorene scaffolds **1**-**3** reported in Scheme 1.[54] The results highlighted that, although only the fluorenone derivative **3** was fluorescent in solution, all three linkers were fluorescent in the solid state. This prompted us to use the three linkers for the fabrication of mixed-ligand MOFs to investigate their

[a] Department of Chemical Sciences, Life Sciences and Environmental Sustainability, University of Parma, Parco Area delle Scienze 17/A, 43124 Parma, Italy. Email: paolo.pelagatti@unipr.it, francesca.terenziani@unipr.it
[b] Department of Chemistry, Università degli Studi di Milano, via Golgi 19, 20133 Milano, Italy.
[c] Department of Materials Science, University of Milano-Bicocca, via Roberto Cozzi 55, 20125 Milano, Italy.
[d] Interuniversity Consortium Chemical Reactivity and Catalysis (CIRCC), via Celso Ulpiani 27, 70126 Bari, Italy.

Electronic Supplementary Information (ESI) available: ^{1}H NMR spectra of the digested MOFs, TGA traces of pristine MOFs, ORTEP drawings, XRPD trace of **PUM310** after activation, views of the catenated cubic cages, BET analysis, absorption and emission profiles of H_2ndca and solid state absorption of ligands **1**-**3**. See DOI: 10.1039/x0xx00000x

luminescent properties in the solid state, making a comparison with the free linkers. In this paper, we analyze the results obtained reacting **1**-**3** with $Zn(NO_3)_2{\cdot}6H_2O$ and 2,6-naphthalenedicarboxylic acid in N,N-dimethylformamide (DMF), under solvothermal conditions. The solid state structures of the three new MOFs (**PUM310**, containing **1**; **PUM310Me$_2$**, containing **2**; **PUM310CO**, containing **3**) and their topologies are described, along with their thermal behavior and luminescent properties in the solid state.

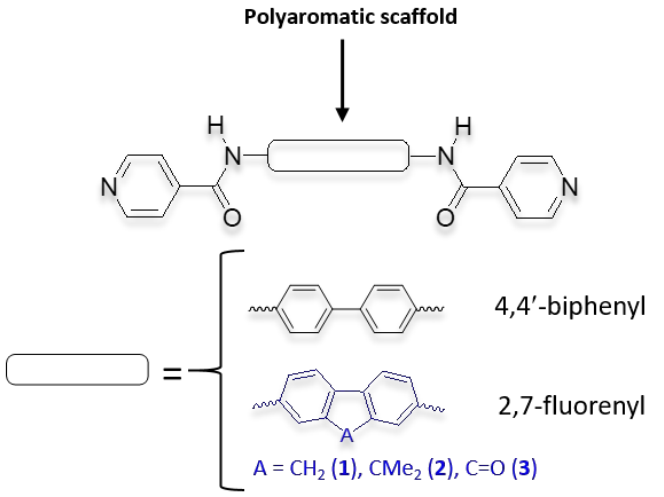

Scheme 1. General structure of bis-isonicotinoyl linkers containing different polyaromatic scaffolds. The 2,7-fluorenyl scaffold contained in the linkers used for the construction of the MOFs described in this work is in blue.

Experimental

Materials and Methods

All reagents and solvents were used as received. The bis-pyridyl-bis-amide ligands 1-3 were synthesized as previously reported.[54]

1H NMR spectra were recorded on a 400 or 300 MHz Bruker instruments after dissolution of the materials in one drop of CF_3COOD (TFA) and dilution with $(CD_3)_2SO$ (DMSO). Chemical shifts are reported in ppm relative to the solvent residual peak of deuterated DMSO (‘H= 2.50). TGA analyses (sample mass approximatively 1-3 mg) were conducted by means of a PerkinElmer TGA8000 instrument, using a Pt-crucible, with a temperature increment of 10 °C/min in the temperature range 25-500 °C. The measurements were performed under ambient pressure with a nitrogen gas flow of 80 mL/min. The maximum temperature was fixed at 500 °C to avoid any damage of the Pt-crucible, due to the presence of metal in the specimen. The elemental analyses were performed by a Thermo Fisher FlashSmart instrument, with gas-chromatographic separation.

Single crystal X-ray diffraction data were collected at Elettra Synchrotron (Trieste, Italy), beamline XRD1.[55] Crystals were directly fished out from DMF and data were collected at 100 K using an Oxford Cryostream system. Beamline spectra (produced by a NdBFe multipole wiggler) were monochromatized to 17.71 keV (0.700 Å) through a Si(111) double crystal monochromator and focused to obtain a beam size of 0.2 × 0.2 mm FWHM at the sample (photon flux 10^{12}–10^{13} ph s^{-1}). Datasets were collected at 100 K (nitrogen stream supplied through an Oxford Cryostream 700) through the rotating crystal method. Diffraction data were indexed, integrated and scaled by using the software CrysAlis.[56] Structures were solved by direct methods using SHELXT[57] and refined by full-matrix least-squares on all F^2 using SHELXL[58] implemented in Olex2.2.[59] For all structures, anisotropic displacement parameters were refined except for hydrogen atoms. Table 1 reports crystal data collection and refinement results. ORTEP diagrams are reported in the ESI. Crystallographic data for the reported structures have been deposited with the CCDC codes 2215000-2215002.

UV-Vis absorption spectra were recorded with a PerkinElmer Lambda650 spectrophotometer; fluorescence measurements were performed with a FLS1000 Edinburgh Instruments Fluorometer. Emission spectra of liquid samples were collected on diluted solutions, with absorbance lower than 0.1. Solutions for spectroscopic measurements were prepared using spectra grade or HPLC solvents.

The spectroscopic analysis of solid samples required a careful preparation of the specimens: a small quantity of solid was ground in a mortar and then deposited mechanically on a quartz plate, creating an extremely thin layer. For absorption measurements, the samples thus prepared were directly placed into the sample holder of the Lambda650 spectrophotometer; absorption spectra were collected in transmission mode, with the light beam directed perpendicularly through the sample, using air as reference. For emission spectra, the thickness of the layers was reduced as much as possible to minimize inner-filter effects, considering the thickness acceptable when the excitation profile of $ndca^{2-}$ (the energy donor) was comparable with the absorption spectrum of pure H_2ndca. In order to prevent the reflected light from propagating along the emission path, a front-face sample holder was used to collect fluorescence spectra of thin layers, which was rotated by 45° with respect to the excitation beam and tilted off the vertical. Moreover, potential artefacts due to scattering and stray light were removed by employing appropriate longpass filters in the emission path (the cut-off wavelength is indicated in the captions of the figures). Corrections for detector sensitivity and excitation intensity were applied to all the fluorescence and excitation spectra.

N_2 adsorption isotherms at 77 K and CO_2 adsorption isotherms at 195 K were collected up to 1 bar using Micromeritics analyser ASAP2020 HD.

Synthesis of PUM310, PUM310CO and PUM310Me$_2$

Syntheses of the coordination networks were conducted under solvothermal conditions dissolving **1**-**3** (0.05 mmol), 2,6-naphthalenedicarboxylic acid (H_2ndca, 0.1 mmol, 21.6 mg) and $Zn(NO_3)_2{\cdot}6H_2O$ (0.1 mmol, 29.7 mg) in 10 mL of DMF at room temperature in a 20 mL screw-capped Pyrex-glass tubes. The mixture was sonicated until complete dissolution of the reagents, then the sealed tube was immersed in a silicon oil bath thermostated at 80 °C, for the time necessary to grow X-

ray quality single crystals. Then the tube was slowly cooled at room temperature, the crystals were filtered off, washed with DMF (2×5 mL). To avoid degradation, the crystals were stored under DMF. Prior to be analysed by ^{1}H NMR and TGA, the crystals were gently passed over a filter paper to remove DMF from the surface of the crystals.

Synthesis of PUM310: Following the general procedure with ligand **1** (40.6 mg). The solution was heated for five days isolating yellow plate crystals. TGA (% weight loss): 27.9%, in the interval 30-100°C, which corresponds to 7 molecules of DMF. Decomposition occurs at temperature > 400°C. Elemental analysis calculated for $C_{64}H_{43}N_5O_{15}Zn_3$·3(DMF): C, 57,03 (56,85); H, 4,20 (3,88); N, 7,29 (7,01), indicative of a partial loss of solvent during storage.

Synthesis of PUM310Me2: Following the general procedure with ligand **2** (43.4 mg). The solution was heated for four days isolating yellow plate crystals. TGA (% weight loss): 16,07%, in the interval 30-250 °C, corresponding to 7 molecules of DMF; decomposition temperature > 400°C. Elemental analysis calculated for $C_{132}H_{93}N_{10}O_{30}Zn_6$·3(DMF): C, 67,24 (66,85); H, 4,56 (4,36); N, 7,23 (7,11), indicative of a partial loss of solvent during storage.

Synthesis of PUM310CO: Following the general procedure with ligand **3** (42.0 mg). The solution was heated for four days isolating orange plate crystals. TGA (% weight loss): 31,09%, in the interval 30-250 °C, corresponding to 8 molecules of DMF; decomposition temperature > 400°C. Elemental analysis calcd for $C_{64}H_{41}N_5O_{16}Zn_3$·4(DMF): C, 56,19 (56,09); H, 4,28 (3,98); N, 7,76 (7,51), indicative of a partial loss of solvent during storage.

Result and Discussion

View Article Online
DOI: 10.1039/D3CE00087G

Synthesis and structural characterization

The three bis-amide-bis-pyridine ligands **1**-**3** were reacted under solvothermal conditions with 2,6-naphthalene dicarboxylic acid (H_2ndca) and zinc nitrate hexahydrate in DMF at 80°C, as depicted in Figure 1.

The reactions with **1** and **3** led to the isolation of yellow and orange crystals, corresponding to **PUM310** and **PUM310CO**, respectively. The two MOFs are isostructural, crystallizing in the *P2$_1$/c* monoclinic space group. The content of the asymmetric units is very similar, differing only for the DMF content. In both cases the asymmetric unit contains three independent Zn^{2+} ions, a **L** (L = **1** or **3**) ligand, three $ndca^{2-}$ anions and a coordinated DMF molecule. A partially occupied DMF molecule H-bonded to an amide NH group was also observed in **PUM310**. Unmodelled residual electron density is ascribable to disordered molecules of DMF included in the cavities of the frameworks of **PUM310** and **PUM310CO**, respectively. The ^{1}HNMR spectra of crystals of **PUM310** and **PUM310CO** digested in a mixture of TFA-d and DMSO-d_6, indicate the presence of about 10 and 8 molecules of DMF, respectively. TGA analysis showed a weight loss percentage of 27.9% and 31.09% in the interval 30-250 °C for **PUM310** and **PUM310CO**, respectively, corresponding to the departure of about 7 and 8 molecules of DMF. Although a perfect counting of the DMF molecules is difficult, we believe that TGA data are more reliable, and then the general formulae of the two MOFs can be indicated as $[Zn_3(\mathbf{1})(ndca)_3(DMF)]_n(DMF)_6$ and $[Zn_3(\mathbf{3})(ndca)_3]_n(DMF)_8$, respectively.

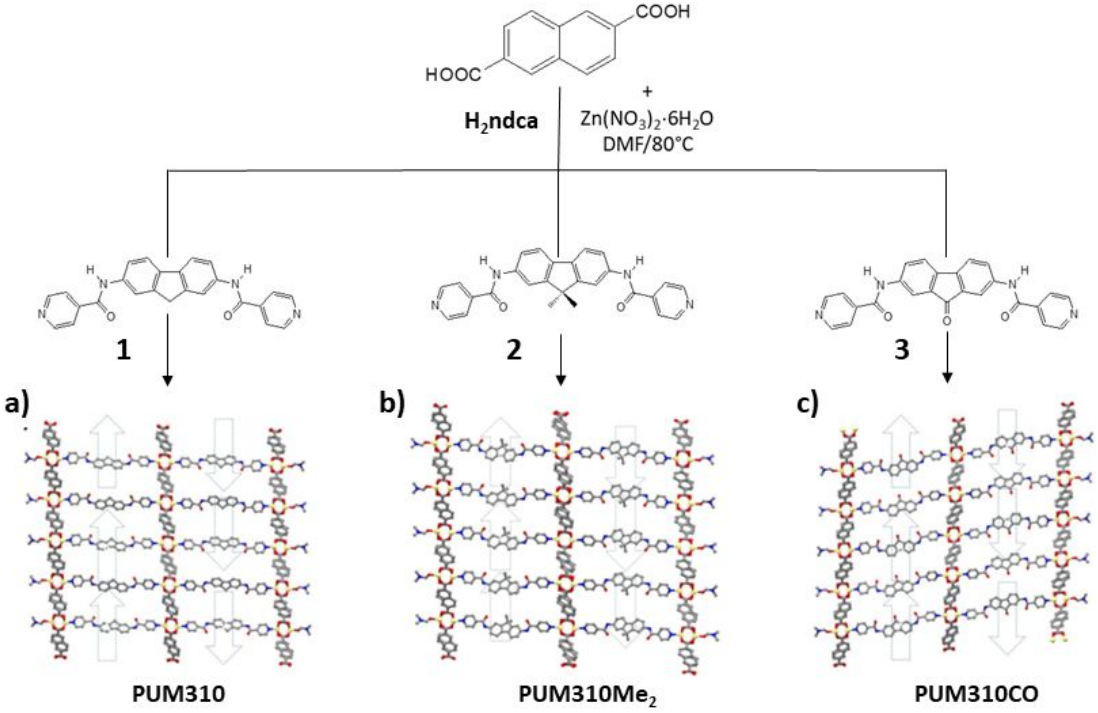

Figure 1 General scheme of the synthesis of a) **PUM310**, b) **PUM310Me$_2$** and c) **PUM310CO**. For each MOF the view along the crystallographic b axis of the framework is reported, highlighting the reciprocal orientation of the fluorenyl ligand (and the amidic moieties) within the same net. Crystallographic disorder has been removed for the sake of clarity.

View Article Online
DOI: 10.1039/D3CE00087G

Decomposition of the frameworks occurred at temperatures higher than 400°C. The reaction with **2** led to **PUM310Me$_2$**, which crystallizes in the $P\bar{1}$ space group and it is isoreticular with **PUM310** and **PUM310CO** (see Figure 2). The content of the asymmetric unit is higher than in the other two cases due to the space group symmetry. Here in fact, there are six metal nuclei, six ndca^{2-} anions each bridging two Zn^{2+} nuclei, two bis-amide ligands, two coordinated DMF molecules and other three modelled molecules of solvent included in the cavities of the framework.

The ^{1}HNMR spectrum of crystals of **PUM310Me$_2$** digested in a mixture of TFA-d and DMSO-d^6 indicates the presence of approximatively 7 molecules of solvent. The approximate general formula is then $[Zn_6(\mathbf{2})_2(ndca)_6(DMF)_2](DMF)_5$. The number of DMF molecules was confirmed by TGA analysis with a weight loss percentage of 16.07% in the interval 30-250 °C. Framework decomposition occurred at temperatures higher than 400 °C. It is worth noting that methyl groups in **2** prevent the net disorder in **PUM310Me2** which is instead evident for **PUM310** and **PUM310CO**. In particular, ligand **3** in **PUM310CO** is heavily disordered with two mutually exclusive orientation of the amide groups, while ligand **1** in **PUM310**, keeps the same orientation of the amide groups. Likewise other MOFs belonging to the PUM series containing ndca^{2-}, in particular **PUM210** and **PUM210F**,[53] the frameworks of **PUM310** and **PUM310CO** contains two different SBUs. One is constituted by a complete paddle-wheel of formula $[Zn_2(COO)_4(\mathbf{L})_2]$ (Figure 2c), where the two metals coordinate four bridged carboxylate groups and two pyridines. The second SBU is a truncated paddle-wheel of formula $[Zn_2(COO)_4(\mathbf{L})(DMF)]$, where an O-coordinated DMF molecule replaces a pyridine (Figure 2b). The coordinated DMF molecule blocks the expansion of the framework which is interrupted after a pass of two ligands **L** (see Figure 1). The two SBUs are part of 2D sheets that form planes where the carboxylate ligands lie. These planes are then bridged by **L** linkers. The three structures show polycatenation, analogous to that found in **PUM210F**[53]. **PUM310** shows channels having dimensions of 17.7 x 12.8 Å^2, the void percentage of the unit cell being 24,8%, corresponding to 2648 Å^3 (calculated by Solvent Accessible Surface function of Mercury), after removal of disorder. **PUM310CO** instead, shows channels having a section of 12 Å x 28 Å, with a unit cell void percentage of 24,3% corresponding to 2532 Å^3 (calculated by Solvent Accessible Surface function of Mercury), after removal of disorder. Finally, **PUM310Me$_2$** has channels of 13 Å x 19 Å, corresponding to a unit cell void volume of 21,4%, equivalent to 2184 Å^3 (calculated by Solvent Accessible Surface function of Mercury), after removal of disorder. Looking at the values of the void volumes of the cells, it turns that functionalization of C9 of the fluorenic core translates into a slight decrease of porosity, with **PUM310** being featured by the highest void volume.

Framework topology

Table 1. Crystal data and structure refinement for **PUM310**, **PUM310CO** and **PUM310Me$_2$**

Identification code	PUM310	PUM310CO	PUM310Me$_2$
Empirical formula	$C_{64}H_{43}N_5O_{15}Zn_3$ ·0.5(C_3H_7NO)	$C_{64}H_{41}N_5O_{16}Zn_3$	$C_{132}H_{93}N_{10}O_{30}Zn_6$·3($C_3H_7NO$)
Formula weight	1354.69	1332.13	2910.67
Temperature/K	100(2)	100(2)	100(2)
Crystal system	monoclinic	monoclinic	triclinic
Space group	P21/c	P21/c	P-1
a/Å	32.28(6)	31.752(2)	17.6312(7)
b/Å	17.76(3)	17.8208(5)	19.4232(4)
c/Å	19.21(3)	19.1271(8)	31.8390(12)
α/°	90	90	104.948(3)
β/°	104.08(5)	105.392(6)	103.585(3)
γ/°	90	90	90.131(3)
Volume/Å^3	10685(31)	10434.8(10)	10216.7(6)
Z	4	4	2
ρcalcg/cm^3	0.842	0.848	0.946
μ/mm^{-1}	0.710	0.699	0.719
F(000)	2768.0	2712.0	2990.0
Crystal size/mm^3	0.08 × 0.06 × 0.02	0.06 × 0.06 × 0.02	0.06 × 0.04 × 0.02
Radiation	synchrotron (λ = 0.700)	synchrotron (λ = 0.700)	synchrotron (λ = 0.700)
2Θ range for data collection/°	4.372 to 59.786	3.454 to 51.888	3.108 to 51.888
Index ranges	-44 ≤ h ≤ 44 -24 ≤ k ≤ 24 -26 ≤ l ≤ 26	-39 ≤ h ≤ 39 -22 ≤ k ≤ 22 -23 ≤ l ≤ 23	-22 ≤ h ≤ 22 -23 ≤ k ≤ 23 -39 ≤ l ≤ 39
Reflections collected	461211	132861	65422
Independent reflections	30220 R_{int}=0.1433 R_{sigma}=0.0703	21230 R_{int}=0.1371 R_{sigma}=0.0778	38133 R_{int}=0.0410 R_{sigma}=0.0709
Data/ restraints/ parameters	30220/ 62/ 603	21230/ 620/ 633	38133/ 0/ 1057
Goodness-of-fit on F^2	1.016	1.467	1.512
Final R indexes [I>=2σ (I)]	R_1 = 0.1008 wR2 = 0.2929	R_1 = 0.1563 wR_2=0.4290	R_1=0.1422 wR_2=0.4017
Final R indexes [all data]	R_1=0.1671 wR_2=0.3656	R_1=0.2076 wR_2=0.4615	R_1=0.1688 wR_2=0.4218
Largest diff. peak/hole /e Å^{-3}	6.20/-1.81	6.01/-2.57	5.09/-2.14

The three structures reported here are built up by 2-periodic 3D layers (that is 2D thick sheets made of three-layers) which are parallel polycatenated (PCAT) to give an overall 3D entangled framework. From a topological point of view the single thick layers are binodal 5,6-connected net with point symbol $(4^{12}\cdot6^3)(4^8\cdot6^2)_2$ and correspond to the topological type 5,6L18. They can be seen as a three-layer section of a **pcu** net whose thickness is of about 58.6, 57.8 and 55.8 Å for **PUM310**, **PUM310CO** and **PUM310Me$_2$**, respectively (computed byToposPro[60]). The polycatenation occurs along the direction perpendicular to the thick layers, that is **a** for **PUM310** and **PUM310CO** and **c** for **PUM310Me$_2$**, with an offset approximately equal to the unit cell axis in that direction

View Article Online
DOI: 10.1039/D3CE00087G

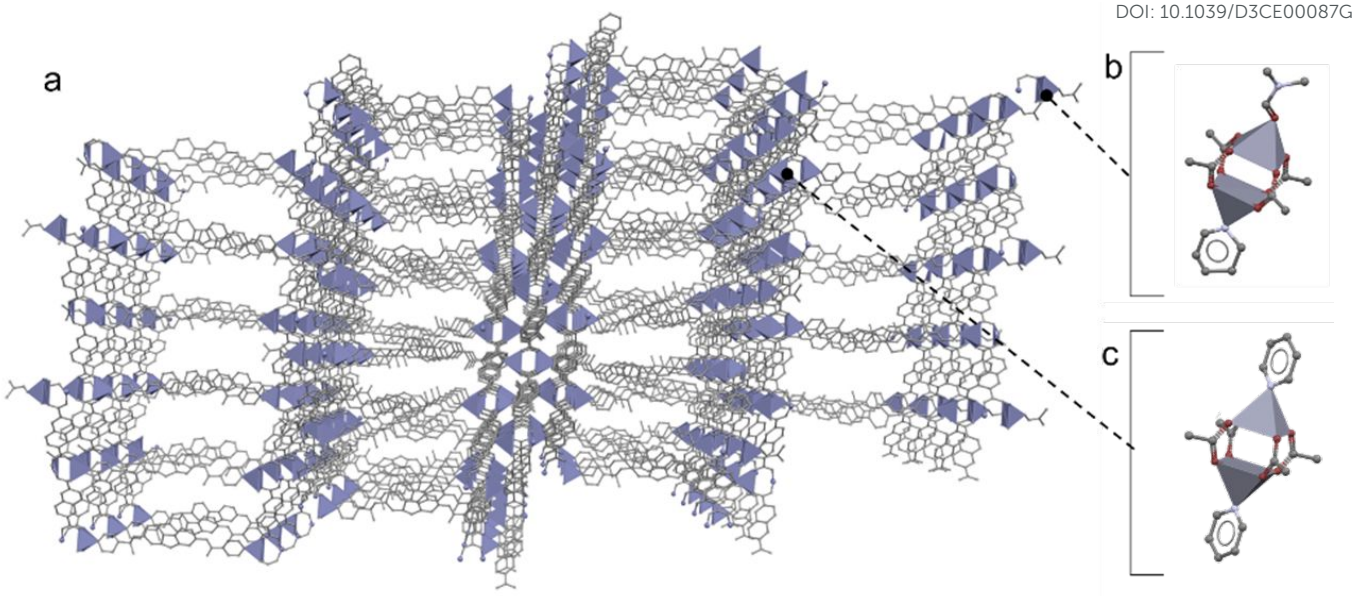

Figure 2. a) Perspective view of the **PUM310** framework along the crystallographic b axis. b-c) Different paddlewheel SBUs are represented as gray polyhedron while the organic ligands are reported in ball and stick style: O red, N blue, C grey.

(ca. 32.28, 31,84 and 31.75 Å, respectively). The PCAT arrays in all three structures are characterized by a degree of catenation of 2 (Doc = 2) and an index of separation of 1 (Is = 1), that is, a single multiple layer is interlaced with other two, the upper and lower nearest neighbors, and to separate in two halves the whole polycatenated framework it is necessary to remove just one layer,[61] see Figure 3.

It results that each cubic cage of the three-layer **pcu** cut (5,6L18) is interlaced with only one cage of the nearest neighbor layer. Differences between the three structures are related to the degree of distortion of the "double cubic cage" of the thick layers, with the more regular and the more distorted ones found, respectively, in **PUM310** and **PUM310Me$_2$**, while **PUM310CO** show only sligth distortion (see Figure 3, right).

This trend seems to follow the steric hindrance of fluorene scaffold and, as a consequence, the relative arrangement of the ligands in the structures is slightly different (Figure S10). The polycatenation shown here (Doc = 2 and Is = 1) is frequently observed for both wavy and thick layers of different topologies,[62,63] however, it is rarely found for layers of the uncommon 5,6L18 topological type.

To the best of our knowledge, this type of thick layer is present in some not polycatenated 2D hybrid perovskites[64–66] and only in two coordination networks previously reported by some of the authors, that is **PUM210F** and **Cu-PUM210F** (CSD refcodes NILFEW and NILFIA[53]). These two networks are strictly related to those reported here, showing the same topology and polycatenation for the layers and differing for the nature of the pillaring ligand (F-bpba). Particularly interesting is the unique structure of **PUM210** (NILFAS), containing the non-fluorinated bpba pillaring ligand and which has previously reported together with NILFEW and NILFIA.[53] In this case the thick 2D motifs are a four-layer **pcu** cut with a thickness of ca. 84.13 Å. The corresponding 2-periodic 3D net is 5,6-connected, with point symbol $(4^{12}\cdot6^3)(4^8\cdot6^2)$ and 5,6L48 topology. The polycatenation occurs along the crystallographic **c** direction with an offset of about 31.06 Å resulting in Doc = 4 and Is = 2 (see Figure 4).

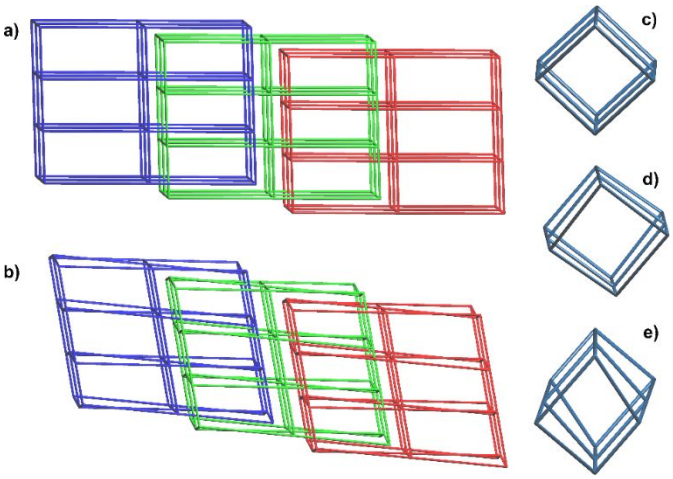

Figure 3: Views of the simplified networks in (a) **PUM310** and (b) **PUM310Me$_2$** showing the three-layer 2D sheets of 5,6L18 topology and the parallel polycatenation with Doc =2 and Is = 1. On the right is shown the distortion of a single "double-cubic cage" in (c) **PUM310,** (d) **PUM310CO** and (e) **PUM310Me$_2$**.

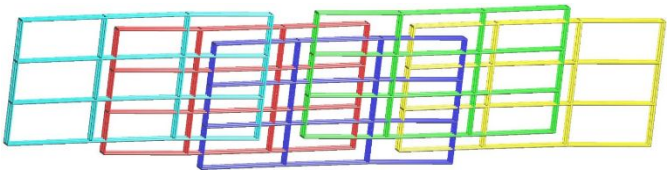

Figure 4: View of the simplified networks in **PUM210** (NILFAS) showing the four-layer 2D sheets of 5,6L48 topology and the parallel polycatenation with Doc =4 and Is = 2.

As can be seen from Figure 4, and at difference from all the other discussed structures, here each cubic cage of a thick layer is interlaced with other two ones belonging to different layers. **PUM210** is the first example of coordination network with the 5,6L48 topology reported so far, and is one of the few examples of polycatenation with Doc and Is higher than, respectively, 2 and 1. The 5,6L48 topology has been found only in some not entangled 2D hybrid perovskites.[64]

The results discussed here confirm the easily occurrence of parallel polycatenation (PCAT) for 2-periodic 3D layers, such as the multiple pillared layer present in the **PUM** coordination networks. Moreover, the variation of the pillaring ligands in terms of length, steric hindrance and chemical functionalization allow the isolation of new topologies and type of polycatenation.

Stability of the framework upon activation

It is known that for application purposes, MOFs must be activated to remove the solvent molecules included in the cavities of their frameworks.[67] This can be a particularly crucial step since removal of the included solvent can be accompanied by framework collapse with consequent closure of the pores. Due to the similarity of the three isolated frameworks, **PUM310** was chosen as representative to study the stability of the frameworks towards DMF removal. A close inspection of the TGA curve of **PUM310** shows that 3 molecules of DMF are lost in the T range 25-110°C (weight loss 12.15%), while other 3 depart between 110 °C and 210 °C (weight loss 11.60%). Finally, between 210 °C and 250 °C a weight loss of 3.96% indicates the departure of an additional DMF molecule. This multistep desolvation profile can be correlated with the increasing degree of interaction between the residual DMF molecules and the framework walls of the MOF. The first loss is ascribed to the departure of the DMF molecules disorderly distributed in the channels, while the other two losses are assigned to the extrusion of the DMF hydrogen-bonded to the framework and coordinated to the Zn of the incomplete SBU, respectively. Thermal activation under dynamic vacuum at a temperature of 100 °C gave back severely damaged crystals, not suitable for single-crystal X-ray analysis, thus indicating the need to follow more gentle techniques. For this reason, a solvent-exchange protocol was followed. This involves the soaking of the crystals in two different low boiling solvents, such as acetone and dichloromethane. With both solvents the soaking was maintained for 24 hours. Subsequently, the crystals were evacuated by simple vacuum at low temperature (see Supporting Information for details). The TGA analysis of the activated crystals still showed a weight loss of 10.33%, corresponding to 2.5 molecules of DMF. Most likely, these correspond to the DMF molecules coordinated to zinc and to those strongly interacting with the amide groups of the framework. The activated crystals were subjected to X-ray diffraction analysis, revealing the formation of a new crystalline phase, hereinafter referred to as **PUM310-a**.

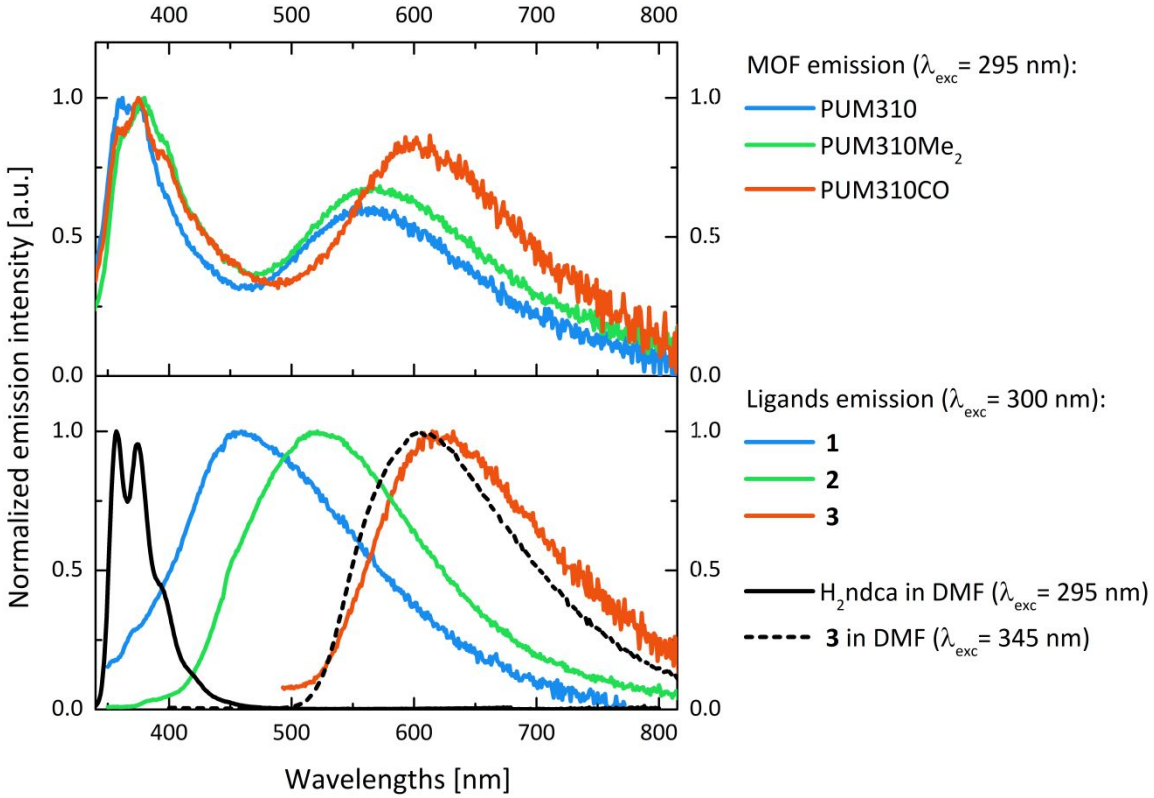

Figure 5 Comparison between emission spectra of the three MOFs and the constituting organic ligands in solid state (**1-3**) or in solution (H_2ndca). Top: emission of **PUM310**, **PUM310Me$_2$** and **PUM310CO** in solid state. Bottom: emission of H_2ndca and **3** solubilized in DMF and of **1-3** in solid state. All the measurements on solid samples were performed using a 330 nm longpass filter. The excitation wavelength is reported in the legend

View Article Online
DOI: 10.1039/D3CE00087G

The single-crystal-to-single-crystal transformation from **PUM310** to **PUM310-a** was accompanied by a relevant reduction of the cell volume, from 10682(31) Å^3 to 3219(3) Å^3, as expected because of the solvent removal. Unfortunately, the framework rearrangement led to damage of the crystals that were no longer suitable for a complete structural resolution. In the attempt to remove completely the included DMF, the soaking times in acetone and dichloromethane were increased to 48 and 72 hours, respectively. The exchanged crystals were then subjected to a heating ramp from 60 °C to 90 °C (within 1 hour). The TGA analysis conducted on the newly activated crystals, hereinafter referred to as **PUM310-a'**, showed a weight loss of 5.89%, corresponding to about one molecule of DMF. We assume that the residual DMF corresponds to that contained in the incomplete SBU. Thermal treatment led again to an excessive degradation of the crystals, which were no longer suitable for single crystal X-ray analysis. However, the XRPD trace of **PUM310-a'** is indicative of a new crystalline phase, as inferable by the comparison with the calculated XRPD trace of **PUM310** (see Figure S11).

To gain indication of the porosity of the three new MOFs, volumetric adsorption analyses were conducted. Activated **PUM310**, **PUM310Me$_2$** and **PUM310CO** do not adsorb N_2 at 77 K (see Figure S12) whilst a CO_2 uptake at 195 K of 3 mmol/g (12% weight) was detected by **PUM310-a'** (see Figure S13). This value leads to about 4 molecules per asymmetric unit. This value is significantly lower than the number of DMF molecules initially included, indicating a rearrangement of the framework upon activation, as already anticipated by XRPD analyses, that likely leads to a significant framework shrinkage.

Luminescence

The four organic ligands employed in the synthesis of **PUM310**, **PUM310Me$_2$** and **PUM310CO** are all fluorescent in the solid state. The spectroscopic properties of **1**, **2** and **3** have been studied in depth in a recent work.[54] The absorption and emission spectra of the H_2ndca ligand in DMF and in the solid state are reported in the Supporting Information (Figure S14).

The three synthesized MOFs have been spectroscopically characterized recording absorption, emission and excitation spectra directly in the solid state. The fluorescence emission spectra are shown in Figure 5 together with the ones of the constituting organic ligands. For each MOF, the bands of the two employed ligands, ndca^{2-} and either **1**, **2**, or **3**, can be recognized in the emission spectra. The MOF emission band related to ndca^{2-} is quite similar to the fluorescence spectrum of H_2ndca in DMF, while the emission spectrum of H_2ndca in the solid state is highly affected by aggregates/excimers formation (see Supporting Information). This is consistent with ndca^{2-} ligands being more spaced in the MOF's structure than in the H_2ndca microcrystals. The emission bands of the fluorene-based ligands in **PUM310** and **PUM310Me$_2$** are almost superimposed and are comparable to pure **2** at the solid state, but strongly red-shifted with respect to pure **1**. The emission band of the fluorenone ligand is practically the same for **PUM310CO**, for **3** as powder and for **3** in DMF solution. The large difference between the emission spectra of **PUM310** and **1** as a pure solid can be justified considering the crystal structure of this bis-isonicotinoyl ligand. From the structural data previously reported,[54] molecules are closer in the crystal structure of **1** than in the crystal structure of **2** or in the corresponding MOF. Additionally, several CH–π interactions directly involving the fluorenyl cores were found in the case of pure **1**, which are absent in the structure of **PUM310** and, as expected due to the presence of two methyl groups in position C9, cannot be formed in the case of **2**.

A remarkable complication when measuring fluorescence emission and excitation spectra of solid samples comes from inner filter effects. The primary inner filter effect is related to a very strong absorption of the incident light by the surface of the sample, that prevents the incoming light from reaching inner parts of the sample; in excitation spectra, this can lead to strong deviations from the absorption profile, even observing minima at the wavelengths where maximum absorption occurs. The second inner filter effect is self-absorption of the emitted light by the sample itself; this plays a major role when a significant overlap between emission and absorption spectra is present, and leads to a "spurious" decrease of the emitted intensity in the spectral region overlapping the absorption band. For these reasons, emission and excitation spectra of solid (or highly concentrated) samples are extremely sensitive to the thickness of the sample. In our measurements on solid samples, we used extremely thin layers, so inner filter effects were minimized. The absorption spectra of the three MOFs and of the constituent organic ligands are reported in Figure 7.

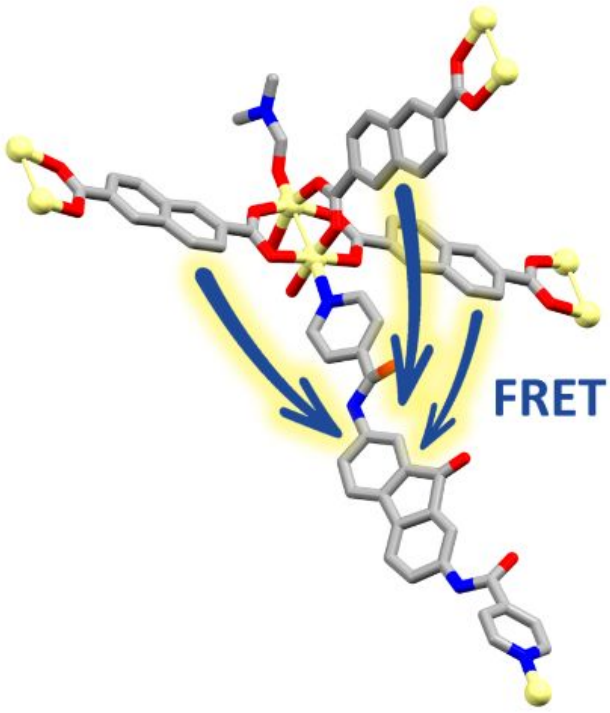

Figure 6 Partial view of a framework node of **PUM310CO**.

View Article Online
DOI: 10.1039/D3CE00087G

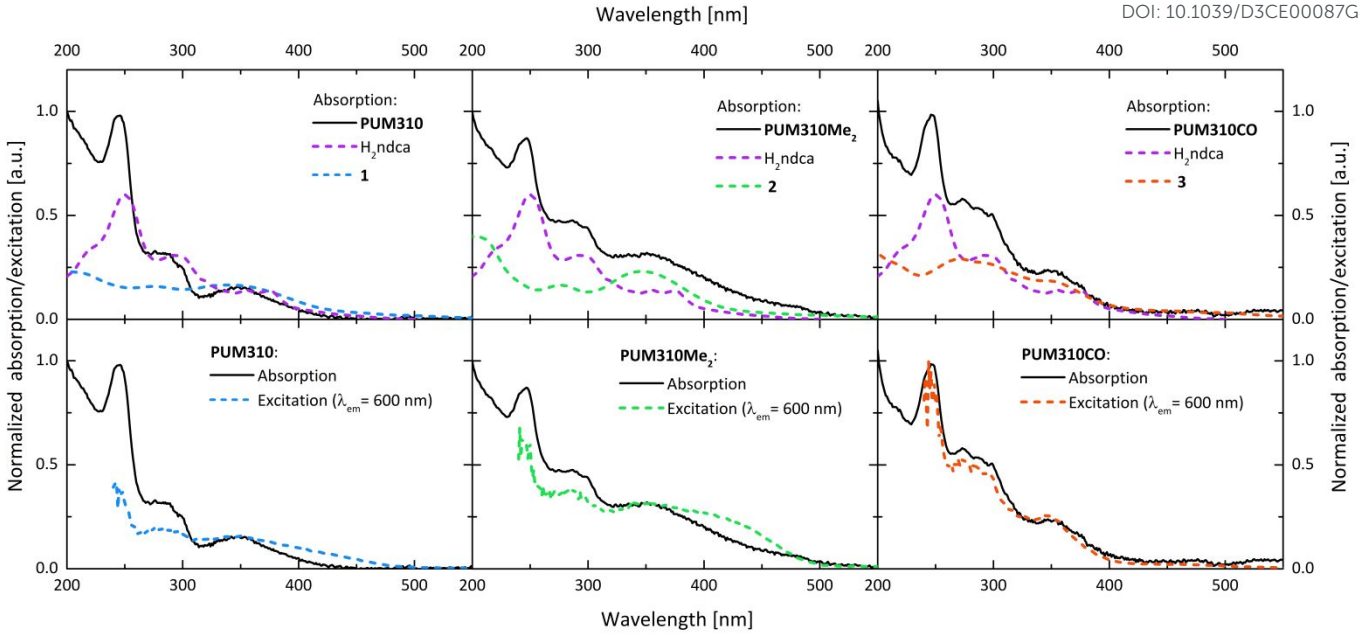

Figure 7 Top: comparison between the absorption spectra of **PUM310**, **PUM310Me$_2$**, **PUM310CO** (continuous black lines), H_2ndca (dashed violet lines), **1** (dashed blue line), **2** (dashed green line) and **3** (dashed orange line). Bottom: comparison between the absorption spectrum of **PUM310**, **PUM310Me$_2$**, **PUM310CO** and the corresponding excitation spectra recorded collecting the acceptor emission at 600 nm.

Contributions from both ndca^{2-} and the corresponding bis-amide-bis-pyridine ligand are clearly present in the absorption spectra of the three materials. The absorption spectra of ligands **1-3** and the emission spectrum of H_2ndca significantly overlap, making them compatible for Förster resonance energy transfer (FRET) (Figure S15). Specifically, ndca^{2-} could act as an excitation energy donor, while the three bis-amide-bis-pyridine ligands could act as acceptors. The structure of the MOFs is compatible with FRET, as the two involved ligands are kept in close proximity to each other by the framework structure. In particular, each bis-amide-bis-pyridine ligand can exchange energy with multiple ndca^{2-} located within the same framework (Figure 6) or in the nearest polycatenated ones.

The selective excitation of the energy donor (ndca^{2-}) is not possible, because of the strong overlap of its absorption bands with those of the other ligands in the MOFs (Figure 7, top panels). Therefore, to verify the occurrence of FRET, we acquired the fluorescence excitation spectra of the MOFs while selectively recording the emission from the acceptor ligand (either **1**, **2** or **3**) at 600 nm (Figure 7, bottom part). The excitation spectra that we obtained for the three MOFs not only display the bands corresponding to the acceptor absorption (either **1**, **2** or **3**), but also the bands corresponding to the donor absorption (ndca^{2-}; very suggestive is the peak at ~250 nm). In the specific case of **PUM310CO**, the relative intensity of the two contributions is the same as in the corresponding absorption spectrum, suggesting a FRET efficiency close to 100%.

Conclusions

Three new frameworks belonging to the PUM series have been obtained by reacting Zn^{2+} ions with 2,6-naphthalenediacrboxylic acid and three diverse bis-pyridine-bis-amide pillars containing differently functionalized fluorene scaffolds. The type of substituent on the C9 carbon of the fluorene moiety has a little effect on the type of final framework, and the three MOFs **PUM310**, **PUM310Me$_2$** and **PUM310CO** are isoreticular. Interestingly, as previously observed by us with other MOFs deriving from the combination of 2,6-naphthalenedicarboxylic acid and biphenyl-based bis-pyridine-bis-amide ligands,[53] the frameworks contain two different types of SBUs, corresponding to complete and truncated paddle-wheel units. The three-dimensionality is then reached by parallel polycatenation. Although potentially microporous, the flexibility of the frameworks leads to a significant shrinkage of the pores upon desolvation, as evidenced by volumetric adsorption analysis. The framework distortion has been partly followed by X-ray diffraction analysis for **PUM310**, but unfortunately the damage of the crystal during solvent removal has prevented a single-crystal-to-single-crystal transformation and then the elucidation of the desolvated structure. The three new MOFs are strongly fluorescent and show FRET from the dicarboxylate dianion to the bis-pyridine linkers, with high efficiencies, close to 100% in the case of **PUM310CO**. These light-harvesting and directional FRET features are promising for multiple sensing applications.

Author Contributions

The manuscript was written through contributions of all authors. All authors have given approval to the final version of the manuscript.

Conflicts of interest

There are no conflicts to declare.

Acknowledgements

Chiesi Farmaceutici SpA is thanked for providing the Bruker D8 Venture diffractometer at the Laboratorio di Strutturistica 'M. Nardelli' of the University of Parma. This work has benefited from the equipment and framework of the COMP-HUB Initiative, funded by the ''Departments of Excellence'' program of the Italian Ministry for Education, University and Research (MIUR, 2018–2022). The Centro Interdipartimentale di Misure "G. Casnati" is thanked for instrument facilities. Alessandro Pedrini (University of Parma) is thanked for BET analyses recording. Dr. Nicola Demitri is thanked for assistance during Elettra Synchrotron data collection.

Funding Sources

MIUR project "Nature Inspired Crystal Engineering" (PRIN2020).

Abbreviations

bpba, bis-pyridine-biphenyl amide;
DMF, N,N-dimethylformamide;
FRET, Förster resonance energy transfer
H_2ndca, 2,6-naphthalenedicarboxylic acid;
PUM, Parma University Materials.

Notes and references

1 H. Li, M. Eddaoudi, M. O'Keeffe and O. M. Yaghi, *Nature*, 1999, **402**, 276–279.
2 H. C. J. Zhou and S. Kitagawa, *Chem. Soc. Rev.*, 2014, **43**, 5415–5418.
3 S. Kitagawa, R. Kitaura and S.-I. I. Noro, *Angew. Chem. Int. Ed*, 2004, **43**, 2334–2375.
4 M. Eddaoudi, D. B. Moler, H. Li, B. Chen, T. M. Reineke, M. O'Keeffe and O. M. Yaghi, *Acc. Chem. Res.*, 2001, **34**, 319–330.
5 O. M. Yaghi, M. O'Keeffe, N. W. Ockwig, H. K. Chae, M. Eddaoudi and J. Kim, *Nature*, 2003, **423**, 705–714.
6 R. B. Lin, Z. Zhang and B. Chen, *Acc. Chem. Res.*, 2021, **54**, 3362–3376.
7 G. Cai, P. Yan, L. Zhang, H. C. Zhou and H. L. Jiang, *Chem. Rev.*, 2021, **121**, 12278–12326.
8 L. Meng, K. Liu, S. Fu, L. wang, C. Liang, G. Li, C. Li and Z. Shi, *J. Solid State Chem.*, 2018, **265**, 285–290.
9 W. Fan, X. Zhang, Z. Kang, X. Liu and D. Sun, *Coord. Chem. Rev.*, 2021, **443**, 213968.
10 S. H. Goh, H. S. Lau and W. F. Yong, *Small*, 2022, **2107536**, 2107536.
11 D. Balestri, D. Capucci, N. Demitri, A. Bacchi and P. Pelagatti, *Materials (Basel).*, 2017, **10**, 1–12.
12 P. Horcajada, T. Chalati, C. Serre, B. Gillet, C. Sebrie, T. Baati, J. F. Eubank, D. Heurtaux, P. Clayette, C. Kreuz, J. S. Chang, Y. K. Hwang, V. Marsaud, P. N. Bories, L. Cynober, S. Gil, G. Férey, P. Couvreur and R. Gref, *Nat. Mater.*, 2010, **9**, 172–178.
13 J. Vaughn, H. Wu, B. Efremovska, D. H. Olson, J. Mattai, C. Ortiz, A. Puchalski, J. Li and L. Pan, *Chem. Commun.*, 2013, **49**, 5724–5726.
14 P. P. Mazzeo, L. Maini, D. Braga, G. Valenti, F. Paolucci, M. Marcaccio, A. Barbieri and B. Ventura, *Eur. J. Inorg. Chem.*, 2013, 4459–4465.
15 D. Capucci, D. Balestri, P. P. Mazzeo, P. Pelagatti, K. Rubini and A. Bacchi, *Cryst. Growth Des.*, 2017, **17**, 4958–4964.
16 J. Yan, T. Liu, X. Liu, Y. Yan and Y. Huang, *Coord. Chem. Rev.*, 2022, **452**, 214300.
17 N. Kulachenkov, Q. Haar, S. Shipilovskikh, A. Yankin, J. F. Pierson, A. Nominé and V. A. Milichko, *Adv. Funct. Mater.*, 2022, **32**, 1–16.
18 P. L. Wang, L. H. Xie, E. A. Joseph, J. R. Li, X. O. Su and H. C. Zhou, *Chem. Rev.*, 2019, **119**, 10638–10690.
19 F. Bianchi, A. Pankajakshan, F. Fornari, S. Mandal, P. Pelagatti, A. Bacchi, P. P. Mazzeo and M. Careri, *Microchem. J.*, 2020, **154**, 1–7.
20 J. De Tovar, F. Rataboul and L. Djakovitch, *Appl. Catal. A Gen.*, 2021, **627**, 118381.
21 Q. Wang, G. Yang, Y. Fu, N. Li, D. Hao and S. Ma, *ChemNanoMat*, 2022, **8**, 1–19.
22 C. G. Piscopo, M. Schwarzer, M. Herrmann, A. Affini, P. Pelagatti, G. Maestri, R. Maggi and S. Loebbecke, *ChemCatChem*, 2016, **8**, 1293–1297.
23 D. Balestri, Y. Roux, M. Mattarozzi, C. Mucchino, L. Heux, D. Brazzolotto, V. Artero, C. Duboc, P. Pelagatti, L. Marchiò and M. Gennari, *Inorg. Chem.*, 2017, **56**, 14801–14808.
24 J. C. Dai, X. T. Wu, Z. Y. Fu, C. P. Cui, S. M. Hu, W. X. Du, L. M. Wu, H. H. Zhang and R. Q. Sun, *Inorg. Chem.*, 2002, **41**, 1391–1396.
25 M. Marimuthu, S. S. Arumugam, D. Sabarinathan, H. Li and Q. Chen, *Trends Food Sci. Technol.*, 2021, **116**, 1002–1028.
26 L. Chen, D. Liu, J. Peng, Q. Du and H. He, *Coord. Chem. Rev.*, 2020, **404**, 213113.
27 F. Fornari, F. Bianchi, N. Riboni, F. Casoli, A. Bacchi, P. P. Mazzeo, P. Pelagatti and M. Careri, *J. Chromatogr. A*, 2022, **1671**, 463010.
28 K. A. White, D. A. Chengelis, M. Zeller, S. J. Geib, J. Szakos, S. Petoud and N. L. Rosi, *Chem. Commun.*, 2009, 4506–4508.
29 R. Li, S. H. Wang, Z. F. Liu, X. X. Chen, Y. Xiao, F. K. Zheng and G. C. Guo, *Cryst. Growth Des.*, 2016, **16**, 3969–3975.
30 L. Maini, D. Braga, P. P. Mazzeo, L. Maschio, M. Rérat, I. Manet and B. Ventura, *Dalt. Trans.*, 2015, **44**, 13003–13006.
31 D. Braga, L. Maini, P. P. Mazzeo and B. Ventura, *Chem. - A Eur. J.*, 2010, **16**, 1553–1559.
32 F. Farinella, L. Maini, P. P. Mazzeo, V. Fattori, F. Monti and D. Braga, *Dalt. Trans.*, 2016, **45**, 17939–17947.
33 A. C. McKinlay, R. E. Morris, P. Horcajada, G. Férey, R. Gref, P. Couvreur and C. Serre, *Angew. Chemie - Int. Ed.*, 2010, **49**, 6260–6266.
34 S. Z. Zhan, M. Li, X. P. Zhou, J. H. Wang, J. R. Yang and D. Li, *Chem. Commun.*, 2011, **47**, 12441–12443.
35 D. Braga, F. Grepioni, L. Maini, P. P. Mazzeo and B. Ventura, *New J. Chem.*, 2011, **35**, 339–344.

36 P. P. Mazzeo, L. Maini, A. Petrolati, V. Fattori, K. Shankland and D. Braga, *Dalt. Trans.*, 2014, **43**, 9448–9455.
37 L. Maini, D. Braga, P. P. Mazzeo and B. Ventura, *Dalt. Trans.*, 2012, **41**, 531–539.
38 J. Rocha, L. D. Carlos, F. A. A. Paz and D. Ananias, *Chem. Soc. Rev.*, 2011, **40**, 926–940.
39 Q. R. Fang, G. S. Zhu, Z. Jin, Y. Y. Ji, J. W. Ye, M. Xue, H. Yang, Y. Wang and S. L. Qiu, *Angew. Chemie - Int. Ed.*, 2007, **46**, 6638–6642.
40 J. An, C. M. Shade, D. A. Chengelis-Czegan, S. Petoud and N. L. Rosi, *J. Am. Chem. Soc.*, 2011, **133**, 1220–1223.
41 J. Perego, I. Villa, A. Pedrini, E. C. Padovani, R. Crapanzano, A. Vedda, C. Dujardin, C. X. Bezuidenhout, S. Bracco, P. E. Sozzani, A. Comotti, L. Gironi, M. Beretta, M. Salomoni, N. Kratochwil, S. Gundacker, E. Auffray, F. Meinardi and A. Monguzzi, *Nat. Photonics*, 2021, **15**, 393–400.
42 J. Perego, C. X. Bezuidenhout, I. Villa, F. Cova, R. Crapanzano, I. Frank, F. Pagano, N. Kratochwill, E. Auffray, S. Bracco, A. Vedda, C. Dujardin, P. E. Sozzani, F. Meinardi, A. Comotti and A. Monguzzi, *Nat. Commun.*, 2022, **13**, 1–10.
43 M. Du, C. P. Li, C. Sen Liu and S. M. Fang, *Coord. Chem. Rev.*, 2013, **257**, 1282–1305.
44 S. Pullen and G. H. Clever, *Acc. Chem. Res.*, 2018, **51**, 3052–3064.
45 B. Qin, X. Zhang, J. Qiu, G. Gahungu, H. Yuan and J. Zhang, *Inorg. Chem.*, 2021, **60**, 1716–1725.
46 B. Parmar, K. K. Bisht, Y. Rachuri and E. Suresh, *Inorg. Chem. Front.*, 2020, **7**, 1082–1107.
47 Z. F. Qiu, S. M. Zhao, Z. H. Xu, Y. Zhao, Z. L. Wang and W. Y. Sun, *Cryst. Growth Des.*, 2021, **21**, 5306–5316.
48 S. S. Chen, S. S. Han, C. B. Ma, W. D. Li and Y. Zhao, *Cryst. Growth Des.*, 2021, **21**, 869–885.
49 P. P. Mazzeo, D. Balestri, A. Bacchi and P. Pelagatti, *CrystEngComm*, 2021, **23**, 7262–7269.
50 D. Balestri, P. P. Mazzeo, R. Perrone, F. Fornari, F. Bianchi, M. Careri, A. Bacchi and P. Pelagatti, *Angew. Chemie Int. Ed.*, 2021, **60**, 10194–10202.
51 D. Balestri, P. P. Mazzeo, C. Carraro, N. Demitri, P. Pelagatti and A. Bacchi, *Angew. Chemie Int. Ed.*, 2019, **58**, 17342–17350.
52 D. Balestri, P. Scilabra, C. Carraro, A. Delledonne, A. Bacchi, P. P. Mazzeo, L. Carlucci and P. Pelagatti, *CrystEngComm*, 2019, **21**, 6365–6373.
53 D. Balestri, I. Bassanetti, S. Canossa, C. Gazzurelli, A. Bacchi, S. Bracco, A. Comotti and P. Pelagatti, *Cryst. Growth Des*, 2018, **18**, 6824–6832.
54 A. Delledonne, M. Orlandini, P. P. Mazzeo, C. Sissa, A. Bacchi, F. Terenziani and P. Pelagatti, *Phys. Chem. Chem. Phys.*, 2022, **24**, 1191–1201.
55 G. . Lausi, A.; Polentarutti, M.; Onesti, S.; Plaisier, J.R.; Busetto, E.; Bais, G.; Barba, L.; Cassetta, A.; Campi and D. Lamba, *Eur. Phys. J. Plus*, 2015, 1–8.
56 Oxford Diffraction, 2008.
57 G. M. Sheldrick, *Acta Crystallogr. Sect. A Found. Crystallogr.*, 2015, **71**, 3–8.
58 G. M. Sheldrick, *Acta Cryst. Sec. C*, 2015, **71**, 3–8.
59 O. V. Dolomanov, L. J. Bourhis, R. J. Gildea, J. A. K. Howard and H. Puschmann, *J. Appl. Crystallogr.*, 2009, **42**, 339–341.
60 V. A. Blatov, A. P. Shevchenko and D. M. Proserpio, *Cryst. Growth Des.*, 2014, **14**, 3576–3586.
61 L. Carlucci, G. Ciani and D. M. Proserpio, *Coord. Chem. Rev.*, 2003, **246**, 247–289.
62 L. Carlucci, G. Ciani, D. M. Proserpio, T. G. Mitina and V. A. Blatov, *Chem. Rev.*, 2014, **114**, 7557–7580.
63 E. V. Alexandrov, V. A. Blatov and D. M. Proserpio, *CrystEngComm*, 2017, **19**, 1993–2006.
64 X. Li, J. Hoffman, W. Ke, M. Chen, H. Tsai, W. Nie, A. D. Mohite, M. Kepenekian, C. Katan, J. Even, M. R. Wasielewski, C. C. Stoumpos and M. G. Kanatzidis, *J. Am. Chem. Soc.*, 2018, **140**, 12226–12238.
65 Z. Xu, W. Weng, Y. Li, X. Liu, T. Yang, M. Li, X. Huang, J. Luo and Z. Sun, *Angew. Chemie - Int. Ed.*, 2020, **59**, 21693–21697.
66 L. Li, X. Liu, C. He, S. Wang, C. Ji, X. Zhang, Z. Sun, S. Zhao, M. Hong and J. Luo, *J. Am. Chem. Soc.*, 2020, **142**, 1159–1163.
67 J. E. Mondloch, O. Karagiaridi, O. K. Farha and J. T. Hupp, *CrystEngComm*, 2013, **15**, 9258–9264.

View Article Online
DOI: 10.1039/D3CE00087G